

Optimisation Studies of Naphthalene Adsorption on Bentonite Clay Impregnated on Chitosan and Surfactant using RSM–CCD, ANN–BP and ANN–PSO Techniques

Olaosebikan Abidoye Olafadehan ^{*1}, Victor Ehigimotor Bello¹, Oluwasola Oribayo¹, Kehinde Olawale Amoo², Adebukola Morufat Bello¹, Queen Oluwatobi Olafadehan³

¹Department of Chemical Engineering, University of Lagos, Akoka-Yaba, Lagos 101017 Nigeria

²Department of Chemical Engineering, Abiola Ajimobi Technical University, Ibadan, Oyo State, Nigeria

³College of Natural Sciences and Mathematics, University of Denver, Denver, Colorado CO 80208 USA

^{*1}Corresponding Author's Email: oolafadehan@unilag.edu.ng

Abstract

The effects of process variables on naphthalene adsorption on bentonite clay–cetyltrimethylammonium bromide (CTAB)–chitosan matrix were investigated in this study. The independent variables are initial concentration (A), adsorbent dosage (B), contact time (C), temperature (D) and pH (E) while the response variable is the % removal of naphthalene. The adsorption process was modelled and optimised using the response surface methodology (RSM)–central composite design (CCD), artificial neural network (ANN)–back propagation (BP) and ANN–particle swarm optimization (PSO) algorithms. The interactive terms of A and B , B and E , C and E , and D and E give a synergistic effect on the adsorption process. On account of p –value, temperature and adsorbent dosage are the most influential single terms. Among the square terms, adsorbent dosage was found to be the most controlling factor while adsorbent dosage and contact time were the most significant interactive factors for the adsorption process. The RSM–CCD, ANN–BP and ANN–PSO aptly modelled and optimised the process variables. However, the ANN–PSO algorithm excelled over the RSM–PSO and ANN–BP owing to its highest R^2 value of 0.9803, least value of the error functions considered and percentage error of validation. Hence, ANN–PSO is projected for the optimisation studies of naphthalene adsorption on the synthesised bentonite clay–cetyltrimethylammonium bromide (CTAB)–chitosan matrix. These approaches enable scalable and data-driven solutions, which minimise costly trial-and-error experiments for treating industrial wastewater contaminated with persistent pollutants of PAHs.

Keywords: Naphthalene adsorption, bentonite clay–CTAB–chitosan matrix, RSM–CCD, ANN–BP, ANN–PSO, error functions

1.0 INTRODUCTION

The steady transition from scanty to copious industrial outfit of different sectorial classifications and global human population growth has paved way for the hike in the releases of harmful pollutants, and its concomitant degradation of the environment (Puszkarewicz and Kaleta, 2020). One of such pollutants with widespread negative impacts on the environment is the polycyclic aromatic hydrocarbons (PAHs), which include naphthalene, anthracene, phenanthrene and pyrene, amongst others. These PAHs have been ranked dangerous owing to their devastating environmental impacts (El-Zahhar and Idris, 2022; Al-Salman *et al.*, 2023; Yemele *et al.*, 2024). Hence, they are placed on a red alert by concerned health related organization like World Health Organization (WHO), International Agency for Research on Cancer (IARC) and European Environment Agency (EEA). Institutes and administrations saddled with the safety of workers like Occupational Safety and Health Administration (OSHA), National Institute for Occupational Safety and Health (NIOSH) and the American Conference of Governmental Industrial Hygienists (ACGIH) have equally branded and listed PAHs as special hazardous substance whose exposure should be at the barest minimum within the working hours (NMAM, 2019; ACGIH, 2010). According to U.S. Environmental

Protection Agency, the international standards of PAHs in wastewater should be within the range of 0.001–0.004 ppm (Law *et al.*, 2022). PAHs are simply organic compounds whose structural framework is mainly the fusion of at least two benzene rings void of substituents (Emoyan *et al.*, 2011). The rings are uniquely positioned in linear and angular posture, which are characterised with hydrogen atom on their outer brim (Batchamen Mougnolet *et al.*, 2022). They are known to be hydrophobic, persistent, non-ionizable, highly toxic, carcinogenic, mutagenic, teratogenic and possess low rate of degradation and low volatility value (Sabah and Ouki, 2017; Okoro *et al.*, 2019; da Costa *et al.*, 2022). Their prevalence in every segment of the environment, especially the aquatic, is traced to anthropogenic activities (Frescura *et al.*, 2020; Alharbi *et al.*, 2023). The classifications of PAHs in terms of molecular weight are categorised as low and high molecular weight. Those with between two and three benzene rings (such as naphthalene and anthracene) are within the bracket of low molecular weight PAHs while those with more than three benzene rings are in the purview of the high molecular weight PAHs like pyrene (Arikan *et al.*, 2022). The combustion of biomass, fossil fuel, wastes from petrochemical and textile industries, vandalization of oil pipeline leading to full scale leakages and unmanaged accidental spills common in some oil producing nations have heightened the menace of PAHs on the environment (Zango *et al.*, 2019).

The regions of Niger Delta in Nigeria are currently bedevilled with severe environment challenges owing to the proliferations of PAHs in aquatic bodies arising from the huge activities of oil exploration, illegal bunkering of oil and poor handling or operation of modular refining (Zulaihah *et al.*, 2020; Taiwo *et al.*, 2021; Iwurie and Okirigbo, 2022). More so, the report of the Nigerian Bureau of statistics in 2020 attests to it (Ike *et al.*, 2022). These aforementioned ominous activities among others have left much effect on sea foods and by extension to humans. Hence, the Niger Delta is on the brink of environmental abyss. The exercise tailored toward cleaning of the affected areas is still ongoing but on a struggling note and inadequate. The presence of polycyclic aromatic hydrocarbons (such as naphthalene and anthracene) in aqueous solution of petroleum wastewaters is evident with their peculiar exasperating properties for two, three and four ring structures (Yakout *et al.*, 2013). Many processes have been employed for the treatment of water contaminated with PAHs like bioremediation (Agarry *et al.*, 2013), sonocatalytic method (Suresh *et al.*, 2022), degradation by oxidation (Tentori *et al.*, 2021), photocatalytic method (Peng *et al.*, 2018), coagulation (Rosinska and Dabrowska, 2018), membrane filtration (Gong *et al.*, 2017; Urbano *et al.*, 2021), and liquid phase plasma method (Kim *et al.*, 2022).

Adsorption process is one of the mass transfer operations currently being employed for the treatment of wastewater containing PAHs due to its simplicity of design, ease of operation, less financial implication and availability of variants of adsorbent materials with high chelating characteristics and adsorptive capacity (Manyangadze *et al.*, 2020; Al-Alam *et al.*, 2020; Xu *et al.*, 2021; Danesh *et al.*, 2021; Emezio *et al.*, 2022; Garbal *et al.*, 2022; Radoor *et al.*, 2022; Avila *et al.*, 2022; Raaj *et al.*, 2022; Sayed *et al.*, 2022; Asadu *et al.*, 2022). The use of natural, synthetic polymeric materials and modified clay minerals in the form of organic–inorganic hybrid clay like bentonite clay–chitosan is considered very potent for the treatment of effluent contaminated with PAHs especially those modified with surfactant with the view of arresting their hydrophobic nature (Soltani *et al.*, 2019; Satouh *et al.*, 2021), as well as for aqueous solutions studded with other forms of pollutants (Gil *et al.*, 2021; Yeo *et al.*, 2023).

The adsorption of PAHs on the active sites of an adsorbent depends on the PAHs' molecular weights, solubility, melting point, boiling point, vapour pressure and logarithmic n-octanol/water partition coefficients (Llyas *et al.*, 2021; Zhao *et al.*, 2023). The other vital process variables

influencing the adsorption of adsorbate on an adsorbent include initial adsorbate concentration, adsorbent dosage, temperature and pH (Atemkeng *et al.*, 2021, Darwish *et al.*, 2022; Prabhahar *et al.*, 2022). Most available studies that had delved into the adsorption of PAHs have not given much attention on the interactive effects of these process variables (Queiroz *et al.*, 2023). The common tool to investigate the interactive effect of process variables, which is sparingly reported in the literature, is the response surface methodology (RSM). The response surface methodology is a compilation of mathematical and statistical methods for experimental design, analysis and evaluation of the interactive effects of process variables aimed at predicting target response and obtaining process optimum condition despite the complexities sometimes involved (Domgas *et al.*, 2023). The use of multivariate statistics techniques like response surface methodology–central composite design (RSM–CCD) and artificial neural network with back propagation algorithm (ANN–BP) is commonly applied due to the fact that it saves time, cost and operates relatively with a handful of experimental runs as against the one factor at a time (OFAT) approach (Dahlan *et al.*, 2022). RSM can model processes effectively with mainly quadratic features and sometimes perform poorly for complex processes which gives room for the use of other modelling tools like ANN. The artificial neural network (ANN) is one of machine learning tools that act like the operation of the biological neural networks embedded in the human brain. The three distinct layers of ANN is associated with weights and biases that enable the network to establish input-output data relationship. The weights and biases values are being updated after each training cycle using algorithms with back propagation (Al–Alam *et al.*, 2024). The high generalisation ability and vast application of ANN in most fields is attributed with the training back propagation algorithm. However, the training algorithms relatively have slow convergence rate and they are usually locked in local optima, which can be averted with the use of meta heuristics algorithms such as particle swarm optimisation algorithm to achieve suitable weights and biases for improved predictability at low computational time (Alizamir and Sobhanardakani, 2018; Nayagam *et al.*, 2023). Hence, for high accuracy of prediction and to achieve optimum condition in any process, hybrid modelling tools are used (Bello and Olafadehan, 2021).

In this study, the process variables of initial concentration, adsorbent dosage, contact time, temperature and pH associated with the adsorption of naphthalene on bentonite clay–cetyltrimethylammonium bromide (CTAB)–chitosan matrix are modelled using RSM–CCD, ANN–BP, and ANN–PSO algorithms. The process variables were equally optimised from the empirical equations developed with the aid of particle swarm optimisation algorithm for design purposes and application in the treatment of effluents from crude oil exploration activities contaminated with organic hydrophobic compounds.

2.0 MATERIALS AND METHOD

2.1 Materials

The materials used in this study include bentonite clay, cetyltrimethylammonium bromide (CTAB), chitosan, Whatman filter paper (125 mmØ) and distilled water. The chemical is analytical grade of naphthalene, obtained from Lobe Chemie, PVT India while the essential reagents are NaOH with molecular weight of 40 g/mol and purity of 98%, supplied by Merck, India; hydrochloric acid of 36.5–38% composition, specific gravity 1.18, ethanol (absolute concentration of 98%), purchased from BDH laboratories, England. All chemicals were not subjected to further treatment. The tools/equipment are weighing balance, mechanical shaker, measuring cylinder, beakers, conical flasks, constant temperature stirrer, pH meter, double Lamp UV–Vi spectrophotometer, 212- μ m sieve, scanning electronic morphology (SEM)–energy dispersive X-ray spectroscopy (EDX), Fourier-Transform infrared spectroscopy (FTIR), X-ray diffraction (XRD) and X-ray fluorescence (XRF).

2.2 Method

2.2.1 Preparation of adsorbent

The adsorbent is a blend of bentonite clay and chitosan treated with surfactant. The bentonite clay was obtained from South West of Nigeria and was transformed from the natural calcium bentonite clay to sodium bentonite clay after undergoing some pre-treatment process to remove unwanted materials (Olafadehan and Bello, 2022). The chitosan was derived from African giant snail (*Archachatina marginata*) shell waste using the chemo-thermal process under optimised condition after undergoing key pre-treatment operations like washing, drying, pulverization and sieving, as reported in the works of Bello and Olafadehan (2021) and Olafadehan *et al.* (2022).

2.2.2 Characterisation of adsorbent

The synthesised adsorbent was characterized in terms of morphological examination, elemental composition, functional group and bonds presents, crystallinity and chemical compositions via scanning electronic morphology (SEM)–energy dispersive X-ray spectroscopy (EDX), (aided by JOEL-JSM 7600F), Fourier-transform infrared spectroscopy (FTIR), (enabled with the use of Nicolet IS10 model device) and X-ray diffraction (XRD) (carried out using Rigaku D/Max-111C X-ray diffractometer) and X-ray fluorescence (facilitated by TEFA ORTEC automatic X-ray F 1610, Maharashtra, India), respectively (Olafadehan *et al.*, 2022).

2.2.3 Batch adsorption experiment

The investigation of the removal of the naphthalene using the synthesized bentonite clay–cetyltrimethylammonium bromide (CTAB)–chitosan matrix as adsorbent was carried out in the batch mode. The preparation of the stock solution involves the dissolution of 5 g of naphthalene in 1000 mL of distilled water and glacier ethanol solution mixed in ratio 3:2 to avert the challenge of incomplete dissolution and loss due to volatilisation (Balati *et al.*, 2015). The remaining concentrations required were prepared by serial dilution. The solution containing the adsorbent was agitated in a mechanical shaker (JP Selecta SKU 3000974) for 45 min while the residual concentration was determined with the use of double lamp UV-Vi spectrophotometer (Thermo/Milton Roy Spectronic 21D) at maximum wavelength of 270 nm for naphthalene. The percentage removal of naphthalene, $\% R_{NT}$, was calculated using Eq. 1.

$$\% R_{NT} = \left(\frac{c_0 - c_e}{c_0} \right) \times 100 \quad (1)$$

where c_0 and c_e are the initial and equilibrium concentration of naphthalene in the aqueous solution respectively (mg/L).

2.2.4 Optimisation of process variables

The process variables were optimised using RSM–CCD, ANN–BP, and ANN–PSO.

2.2.5 Response surface methodology–central composite design (RSM–CCD)

The design of experiment adopted for the single component adsorption system was the central-composite design (CCD) using design expert software to achieve the optimum and viable conditions of the process variables for efficient adsorption of naphthalene. The factors considered are initial concentration (A), adsorbent dosage (B), contact time (C), temperature (D) and pH (E) while the response variable is the % removal of naphthalene. The parameters were adjusted in accordance with the settings of experimental design involving five process variables with five (5) levels as depicted in **Table 1**. With the aid of Design Expert V13.0 (Stat-Ease, Inc., Minneapolis, MN, USA), the response surface methodology generates a second order quadratic empirical model that correlates the process variables and the response, which is given in Eq. 2.

$$Y = \alpha_0 + \sum_{i=1}^k \alpha_i X_i + \sum_{i=1}^k \sum_{j=1}^k \alpha_{i,j} X_i X_j + \sum_{i=1}^k \alpha_{i,i} X_i^2 + \delta \quad (2)$$

where Y represents the response known as dependent variable; α_0 the constant coefficient, α_i , $\alpha_{i,i}$, $\alpha_{i,j}$ the coefficients for linear, quadratic and interactive effects respectively, X_i , X_j the independent variables, and δ the error.

Table 1: Factors range for the design of experimental range and levels for the single component system

Control factors	$-\alpha (-2)$	-1	0	+1	$+\alpha (+2)$
Initial concentration, A (mg/L)	15	30	45	60	75
Adsorbent dosage, B (g)	0.25	0.5	0.75	1	1.25
Contact time, C (min)	15	30	45	60	75
Temperature, D (°C)	35	50	65	80	95
pH, E	3	5	7	9	11

The ANN is indeed the predominant artificial intelligence used for correlating the input-output data. The algorithm determinately captures the operation of the nervous system and the human brain (Hussain *et al.*, 2022). The reports from the literature widely regard the ANN as a reputable tool for mapping linear and non-linear input-output data marked as either simple or complex (Afroozeh *et al.*, 2018; Moreno and Salazar, 2018). The ANN algorithm is essentially made up of three layers consisting of neurons acting as processing unit knitted together by weights and biases accompanied by selected activation functions for transfer of processed data (Asfaram *et al.*, 2016). The number of the input and output layers is directly related to the number of input and output variables respectively while that of the hidden layer depends largely on trial-and-error procedures to arrive at a suitable learning architecture. The input layer receives the input variables in form of normalized values to avoid negative scale effect. The received values are then ushered to the hidden layers after being weighted and sum with a constant term as bias, which aid quick convergence of results at the output layer (Chittoo and Sutherland, 2020). The cycle continues by updates in weights facilitated by the chosen activation function and back propagation training algorithm, until a minimum possible error value between the predicted and actual data is achieved (Ganesapillai *et al.*, 2022; Faisal *et al.*, 2022). The relationship between the inputs and the forecasted outputs is simply described by Eq. 3 (El-Hanandeh *et al.*, 2021).

$$y = \sum_{i=1}^n \omega_i \varphi_i(x) + \tau_i \quad (3)$$

where y is the predicted output, n the number of neurons in the hidden layer, $\varphi_i(x)$ the non-linear activation such as tangent sigmoid (tansig), log-sigmoid (logsig) and linear (purelin), ω_i and τ_i the weights and biases respectively. Models generated using artificial intelligence usually gives high prediction accuracy resulting to close proximity between the actual experimental values and the predicted values (Okoji *et al.*, 2021).

2.2.6 Particle swarm optimisation

The particle swarm optimisation (PSO) is credited to Eberhart and Kennedy (1995). This optimization technique is a heuristic and population-based stochastic algorithm that mimics the social behaviour of animals typically flocking birds and swarm of insects (Wang *et al.*, 2022; Karri and Sahu, 2018). It is simply a numerical technique, which is based on the motion of virtual particles assumed as each intelligent social animals and the collection called swarm exploring a space within a multidimensional space to locate a suitable point as the minimum or maximum of an optimisation problem. It also works on the premises that each particle flies through the

multidimensional space, adjusting its position in every step with individual consciousness and that of other neighbours toward achieving a collective optimum solution (Rossides *et al.*, 2021). The expressions that represent the update of the velocity and position of the particles in the N-dimensional space is given in Eqs. 4 and 5 respectively (Yadav and Roy, 2023).

$$V_i^{k+1} = wV_i^k + c_1r_1(P_{best,i}^k - P_i^k) + c_2r_2(G_{best,i}^k - P_i^k) \quad (4)$$

$$P_i^{k+1} = P_i^k + V_i^{k+1} \quad (5)$$

where the superscript k is the number of iterations, and $i=1, 2, \dots, N$; N indicating the swarm population or size. V_i^k and P_i^k are the respective initial velocity and position of the particles, V_i^{k+1} and P_i^{k+1} are the updated velocity and position respectively of the particles, c_1 and c_2 are regarded as the cognitive and social parameters that indicate the respective extent of local search and global, w is the weight that reflects the initial velocities of the particles, $P_{best,i}^k$ is best known position of each particle while $G_{best,i}^k$ is the best position of the entire swarm, r_1 and r_2 are random numbers at the interval of 0 to 1. The PSO algorithm is easy to implement, has limited number of parameters, simple to calculate and is less dependent on the set of initial points. Detailed information can be found in the works of Satyobroto (2011), and El-Shorbagy and Hossaniem (2018).

2.2.7 ANN-PSO algorithm

For the ANN-PSO hybrid algorithm, the particle swarm algorithm replaces the role of Levenberg-Marquardt algorithm such that each particle within the poll of populations identifies with the variables associated with the fitness function in order to achieve optimum value of weights and biases for the purpose of maximisation or minimisation (Shariati *et al.*, 2019). The update of weights and biases at any instance is a reflection of the change in velocity and position of the swarm of particles in the N-dimensional space of operation. The ANN-PSO algorithm is succinctly illustrated with the flowchart shown in **Figure 1**.

2.2.8 Error functions

The predictive accuracy of the regression models can be performed via computing the various error functions, given in our previous studies (Olafadehan *et al.*, 2025), which are used to compare the experimental % removal of naphthalene, $Y_{i,e}$, with the corresponding predicted values, $Y_{i,p}$.

3.0 RESULTS AND DISCUSSION

3.1 Characterisation and physicochemical properties of adsorbent

The chitosan and adsorbent matrix were characterised in terms of the morphology, identification of bonds and chemical properties, and elemental composition are reported in details elsewhere (Olafadehan *et al.*, 2023). The physiochemical characteristics of bentonite clay-cetyltrimethylammonium bromide (CTAB)-chitosan matrix such as specific gravity, moisture content, bulk density, particle density, porosity, tapped density, Hauser ratio, iodine number, pore volume, pHzpc, BET surface area, cation-exchange-capacity (CEC), Barrett-Joyner-Halender (BJH) pore diameter, total pore volume, micro pore volume and swell/degree of expansivity are highlighted in **Table 2**.

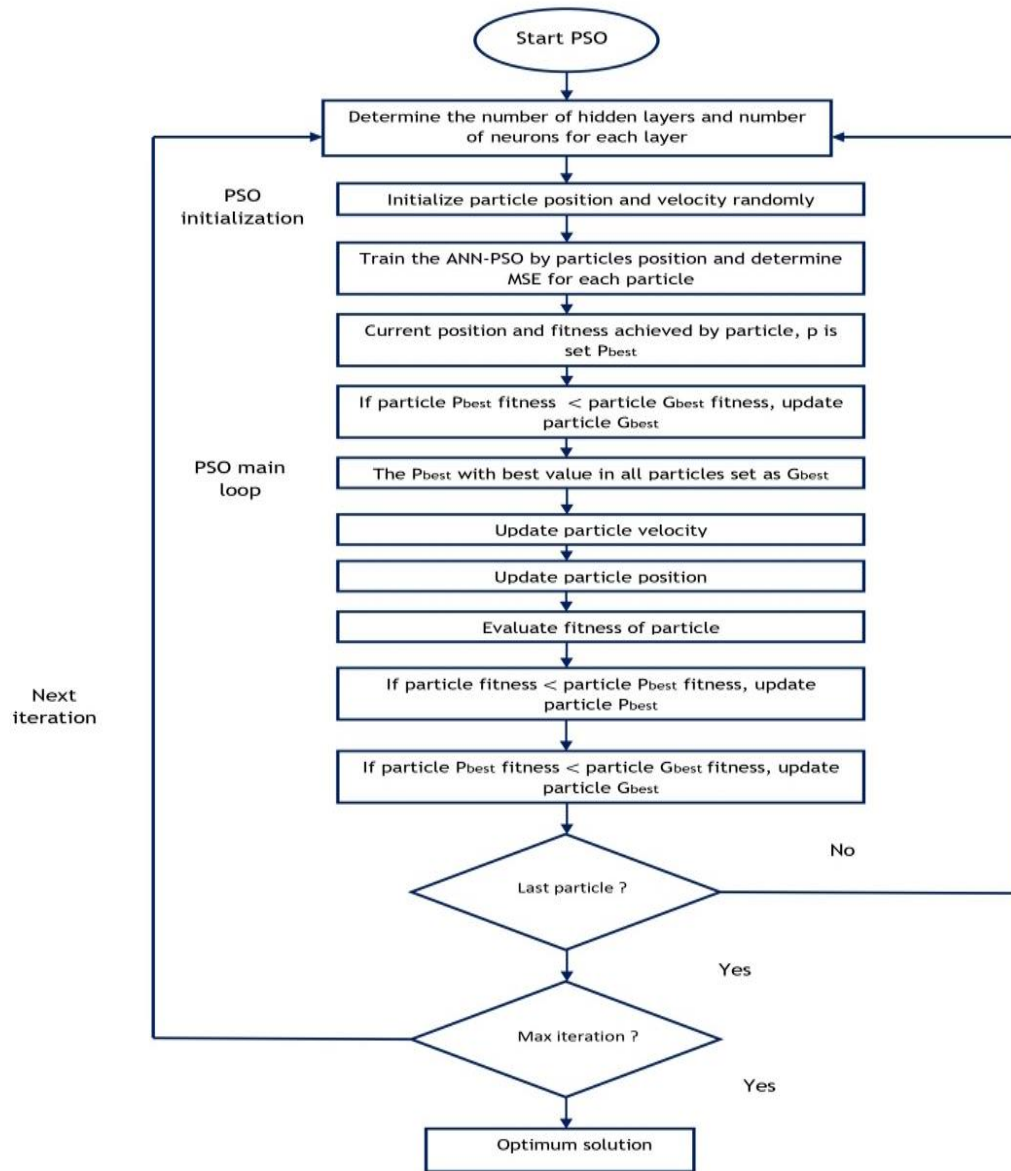


Figure 1: ANN-PSO flowchart

3.2 Response surface methodology (RSM)

Table 3 displays the coefficients estimation for the % removal of naphthalene. The variance inflation factor (VIF) is a term that quantifies the multi-collinearity intensity in the model. In **Table 3**, its values are approximately 1 for all the factors investigated, which is indicative of the fact that these factors are orthogonal and no significant multi-collinearity was observed for all factors under consideration (Bieda *et al.*, 2023). For the fit statistics carried out for % removal of naphthalene, the coefficient of determination, R^2 , was obtained as 0.9552. Conventionally, R^2 value greater 0.9 is adjudged to be a good fit (Azeez *et al.*, 2022). The adjusted R^2 was calculated accordingly as 0.8737. Also, the variation between predicted R^2 and the adjusted R^2 is less than 0.4 for the adsorption of naphthalene. The profound closeness translates to a reasonable agreement (Azhar-ul-Haq *et al.*, 2022).

Table 2: Physiochemical properties of the produced bentonite clay–CTAB–chitosan matrix adsorbent

S/No.	Parameters	Values
1	Specific gravity	0.7179
2	Moisture content (%)	3.04
3	Bulk density(g/cm ³)	0.8367
4	Particle (true) density (g/cm ³)	3.7397
5	Porosity	0.7557
6	Tapped density	0.9136
7	Hausner ratio	1.0919
8	Iodine number (mg/g)	1682
9	Pore (void) volume	0.8272
10	pH _{zpc}	7.20
11	BET surface area(m ² /g)	1668.00
12	Methylene blue surface area (m ² /g)	1,984.05
13	Cation exchange capacity (millieq/100g)	4840
14	Barrett-Joyner-Halender (BJH) pore diameter (Å)	20.82
15	Total pore volume (cm ³ /g)	0.8682
16	Micro pore volume (cm ³ /g)	0.3219
17	Swell/degree of expansivity (%)	97.76

Table 3: Coefficients estimation for quadratic model of % removal of naphthalene

Factor	Coefficient estimate	Df	Standard error	95% CI Low	95% CI High	VIF
Intercept	82.22	1	0.9608	80.11	84.34	
<i>A</i>	1.06	1	0.4917	-0.0242	2.14	1.0000
<i>B</i>	-2.09	1	0.4917	-3.18	-1.01	1.0000
<i>C</i>	0.0087	1	0.4917	-1.07	1.09	1.0000
<i>D</i>	-3.06	1	0.4917	-4.15	-1.98	1.0000
<i>E</i>	1.90	1	0.4917	0.8226	2.99	1.0000
<i>AB</i>	1.93	1	0.6022	0.6072	3.26	1.0000
<i>AC</i>	0.4074	1	0.6022	-0.9180	1.73	1.0000
<i>AD</i>	-1.67	1	0.6022	-3.00	-0.3451	1.0000
<i>AE</i>	-0.1964	1	0.6022	-1.52	1.13	1.0000
<i>BC</i>	-3.94	1	0.6022	-5.26	-2.61	1.0000
<i>BD</i>	-1.44	1	0.6022	-2.77	-0.1193	1.0000
<i>BE</i>	2.52	1	0.6022	1.19	3.84	1.0000
<i>CD</i>	-0.6129	1	0.6022	-1.94	0.7125	1.0000
<i>CE</i>	2.57	1	0.6022	1.24	3.89	1.0000
<i>DE</i>	1.59	1	0.6022	0.2606	2.91	1.0000
<i>A</i> ²	1.48	1	0.4448	0.5002	2.46	1.02
<i>B</i> ²	-2.10	1	0.4448	-3.08	-1.13	1.02
<i>C</i> ²	0.0476	1	0.4448	-0.9313	1.03	1.02
<i>D</i> ²	0.8364	1	0.4448	-0.1425	1.82	1.02
<i>E</i> ²	1.17	1	0.4448	0.1875	2.15	1.02

Table 4 shows the fit of statistics for the adsorption process.

Table 4: Fit of statistic for naphthalene adsorption on the matrix adsorbent

Statistic	Value
Standard Deviation	2.41
Mean	83.29
C.V. %	2.89
R^2	0.9552
Adjusted R^2	0.8737
Predicted R^2	0.5686
Adeq Precision	16.2431

The measure or degree of signal to noise ratio is known as adequate precision (Adeq Precision). The recorded value for naphthalene adsorption was 16.2431, which deciphers that the model is apt to navigate the design space since it is greater than 4, which is the least desirable value (Nguyen *et al.*, 2022). The coefficient of variation (CV), also regarded as normalized root-mean square deviation (NRMSE), describes the ratio of standard error in predicting the mean value of the experimental response and it measures the repeatability of the model. The low value of CV obtained as 2.89 for naphthalene adsorption implies that the experiment was carried out with high precision. It equally gives an impression of high reliability and reproducibility (Onukwuli and Nnanwube, 2022).

The developed prediction equation for the adsorption process expressed in terms of percentage removal of naphthalene ($\% R_{NT}$) is given in Eq. 6.

$$\begin{aligned} \% R_{NT} = & 129.25391 - 0.460702 A + 55.98945 B + 0.265192 C - 0.311945 D - 13.89843 E \\ & + 0.515367 AB - 0.001811 AC - 0.007425 AD - 0.006546 AE - 1.04987 BC - 0.385254 BD \\ & + 5.03183 BE - 0.002724 CD + 0.08515 CE + 0.052868 DE + 0.006574 A^2 - 33.66295 B^2 \\ & + 0.000212 C^2 + 0.00371 D^2 + 0.2916 E^2 \end{aligned} \quad (6)$$

The essence of the model developed in Eq. 6 is to enable predictions about $\% R_{NT}$ for the specified levels of each process variables. For the single effect, A , D , and E show an antagonistic effect on the $\% R_{NT}$ while B and C provide a synergetic effect due to their associated negative and positive signs respectively. The interaction of initial concentration and adsorbent dosage (AB), initial concentration and pH (AE), adsorbent dosage and pH (BE), contact time and pH (CE) and temperature and pH (DE) provides a synergetic effect while the other interactions were antagonistic. The square factors of initial concentration, A^2 , of contact time, C^2 , of temperature, D^2 , and of pH, E^2 , show synergistic effects while the square factor of adsorbent dosage, B^2 , show antagonistic effect on the % removal of naphthalene.

Table 5 shows the results of the analysis of variance (ANOVA) for the response ($\% R_{NT}$) in the adsorption process. The ANOVA test is usually carried out to study the influence of all process variables on the design variables. It is also used alongside with the Fisher variance ratio (F) and significance probability, p , value to ascertain the significance of the model equation and terms embedded in the model developed. The results present that the developed model with large F -values (Fisher variance ratio) of 11.72 with corresponding p -values of < 0.0001 for % removal of naphthalene is regarded as more significant and translates that the model's terms are relevant since $p < 0.05$ (Nagababu *et al.*, 2022). It is also worthy of note that the lack of fit associated with pure error for percentage removal for naphthalene recorded a value of 0.4257 indicating

that the lack of fit is not significant. Equally, the chance of reaching this high value of F -value could result due to noise is 83.59% for the percentage removal of naphthalene (Tai *et al.*, 2021). On account of the p -value (< 0.05), the adsorbent dosage, temperature and initial pH solution are significant while initial concentration and adsorption contact time were statistically not significant for the single term factors. For the interactive terms, initial concentration and adsorbent dosage (AB), initial concentration and temperature (AD), adsorbent dosage and contact time (BC), adsorbent dosage and pH (BE) and contact time and pH (CE) were significant for the interactive terms. The square terms of initial concentration, A^2 , of adsorbent dosage, B^2 , of temperature, D^2 , and of initial pH solution, E^2 , were statistically significant while the square terms of contact time, C^2 , was not statistically significant.

Table 5: Analysis of variance (ANOVA) for quadratic model of naphthalene removal using bentonite clay–CTAB–chitosan adsorbent

Source	Sum of Squares	Df	Mean Square	F -value	p -value	
Model	1360.23	20	68.01	11.72	< 0.0001	Significant
A (initial concentration)	26.87	1	26.87	4.63	0.0545	
B (adsorbent dosage)	105.24	1	105.24	18.14	0.0013	
C (contact time)	0.0018	1	0.0018	0.0003	0.9861	
D (temperature)	225.28	1	225.28	38.83	< 0.0001	
E (pH)	87.08	1	87.08	15.01	0.0026	
AB	59.76	1	59.76	10.30	0.0083	
AC	2.66	1	2.66	0.4578	0.5126	
AD	44.65	1	44.65	7.70	0.0181	
AE	0.6170	1	0.6170	0.1063	0.7505	
BC	248.00	1	248.00	42.74	< 0.0001	
BD	33.39	1	33.39	5.76	0.0353	
BE	101.28	1	101.28	17.45	0.0015	
CD	6.01	1	6.01	1.04	0.3307	
CE	105.55	1	105.55	18.19	0.0013	
DE	40.25	1	40.25	6.94	0.0233	
A^2	64.17	1	64.17	11.06	0.0068	
B^2	129.85	1	129.85	22.38	0.0006	
C^2	0.0666	1	0.0666	0.0115	0.9166	
D^2	20.52	1	20.52	3.54	0.0868	
E^2	39.91	1	39.91	6.88	0.0237	
Residual	63.83	11	5.80			
Lack of Fit	21.58	6	3.60	0.4257	0.8359	not significant
Pure Error	42.24	5	8.45			
Cor Total	1424.05	31				

The plot of predicted % removal of naphthalene versus actual (experimental) values is depicted in **Figure 2**. Herein, the data points are reasonably spread around the straight line, which indicates an excellent correlation the predicted and experimental values of % removal of naphthalene.

3.3 Two-dimensional interactions of process variables

Figures 3a–3d show the 2-dimensional interactions of the process variables for % removal of naphthalene. The spherical, elliptical and curvature shapes portend a reasonable degree of

interaction of the process variables involved in the adsorption of naphthalene on the prepared bentonite clay–cetyltrimethylammonium bromide (CTAB)–chitosan matrix.

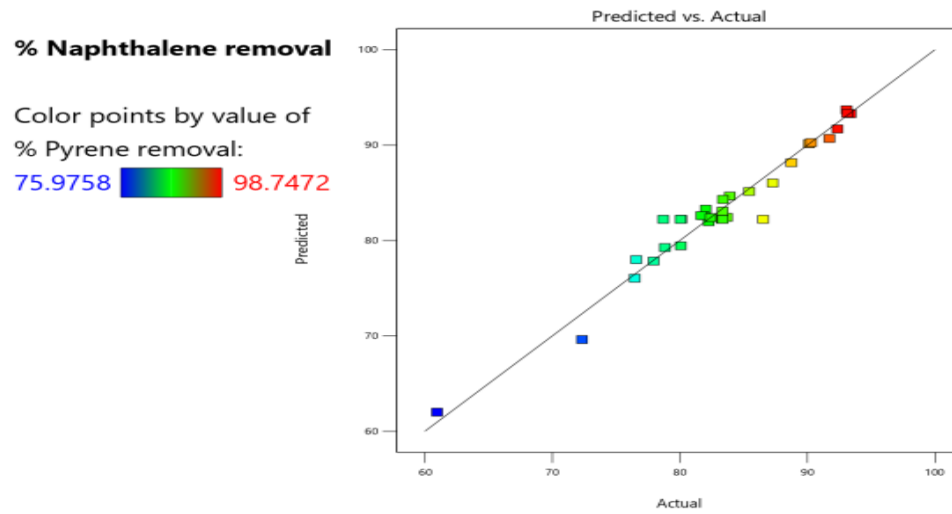


Figure 2: Experimental values versus RSM predicted values of % removal of naphthalene

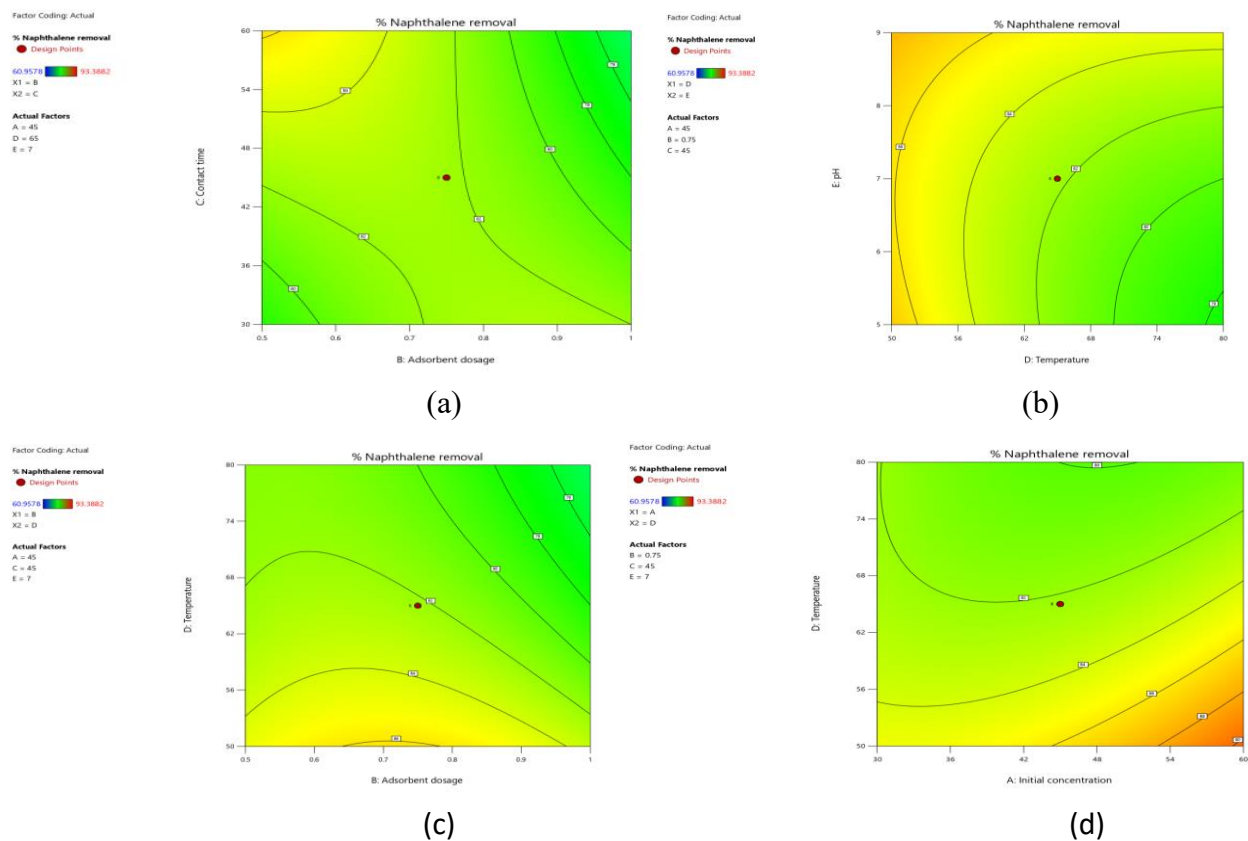


Figure 3: Two-dimensional diagram of the interaction of (a) contact time and adsorbent dosage, (b) initial pH of solution and temperature, (c) temperature and adsorbent dosage, and (d) initial concentration and temperature

3.4 Three-dimensional interactions of process variables

Figures 4a and 4b depict the respective three-dimensional diagram of the interaction of contact time and adsorbent dosage, and initial pH of solution and temperature. In Figure 4a, other factors (initial concentration = 45 mg/L, temperature = 65°C and pH = 7) were held constant. Both interacting factors exhibit a synergetic effect on the response (% removal of naphthalene). It is observed that the percentage removal of naphthalene increases rapidly as the contact time

and adsorbent dosage increase. This could be attributed to the availability of more active sites and sufficient contact time for the adsorbate uptake (Li *et al.*, 2022). The interaction of initial pH of solution and temperature gave a contrasting effect on the response. There was a sharp increase in the percentage removal of naphthalene as the pH increases while a slight decrease was observed as the temperature increases, keeping other factors constant (initial concentration = 45 mg/L, adsorbent dosage = 0.75 g and contact time = 45 min) as depicted in **Figure 4b**. The slight decrease with temperature portends that the adsorption process is favoured at low temperature. A similar result is reported by Albayati and Kalash (2020). The increase with pH suggests the effect of deprotonation of the functional groups associated with chitosan in the adsorbent matrix.

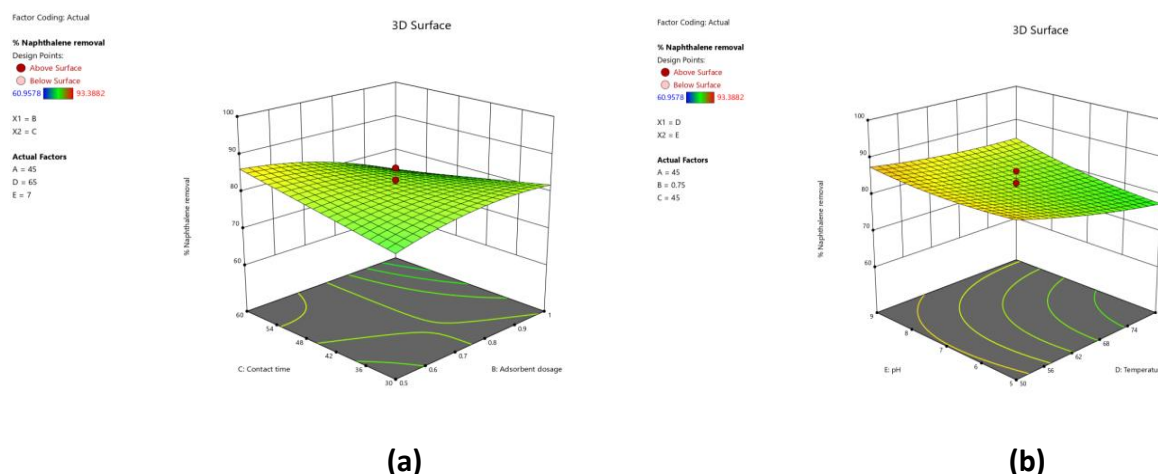


Figure 4: Three-dimensional diagram of the interaction of (a) contact time and adsorbent dosage, and (b) initial pH of solution and temperature

Figures 5a and 5b show the three-dimensional diagram of the interaction between temperature and adsorbent dosage with the inclusion of the effect of initial concentration and temperature of adsorption. **Figure 5** shows a similar trend with **Figure 4**. The interaction of temperature and adsorbent dosage displayed a converse effect on the percentage removal of naphthalene, as depicted in **Figure 5a**. As the adsorbent dosage increases while the temperature decreases, the percentage removal of naphthalene increases on the premises that other factors remained constant (initial concentration = 45 mg/L, contact time = 45 min and pH = 7). With the values of 0.75 g of adsorbent dosage, 45 min of contact time and initial pH solution held constant, the interaction of initial concentration and temperature on the amount of naphthalene uptake is depicted in **Figure 5b**. The effect clearly illustrates a reasonable degree of the naphthalene removed as the initial concentration increases with a corresponding decline in temperature. This is an indication that the percentage removal of naphthalene thrives more at low temperature, relatively high pH value, adsorbent dosage and increased period of contact between the adsorbate/adsorbent systems.

3.5 Artificial neural network (ANN)

The ANN algorithm was carried out in a MATLAB environment (MATLAB 2022a, MathWorks, Inc, MA, USA). The data were normalized to avoid the effect of wide range of parameters involved; to avert the problem of overfitting and to give room for the training of the network to reach convergence with least-mean square error. The appropriate or optimized architectural network was obtained. That is the suitable number of neurons or hidden layers, activation function for the input and output layer and the training algorithms with the least training and validation error were ascertained. The data was split into three parts for training (75%), testing (15%) and

validation (10%). Ten hidden layers, tansig activation function for both input and output layer trained with Levenberg-Marquardt (trainlm) algorithm characterized the optimized network, which produced the least-mean square (MSE) value of 1.33 as depicted in **Figure 6**.

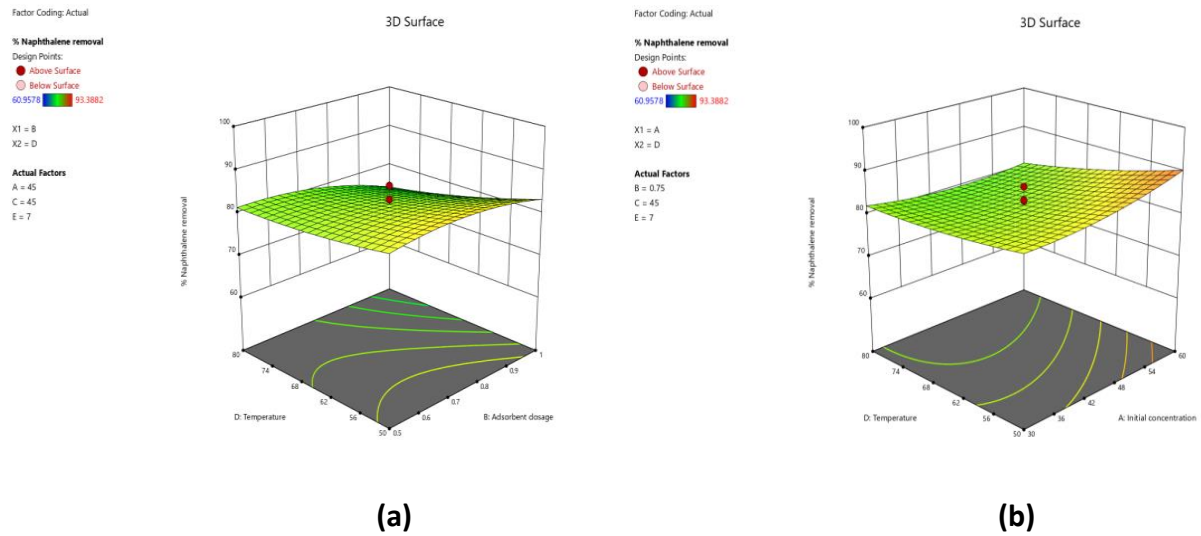


Figure 5: Three-dimensional diagram of the interaction of (a) temperature and adsorbent dosage, and (b) initial concentration and temperature of naphthalene

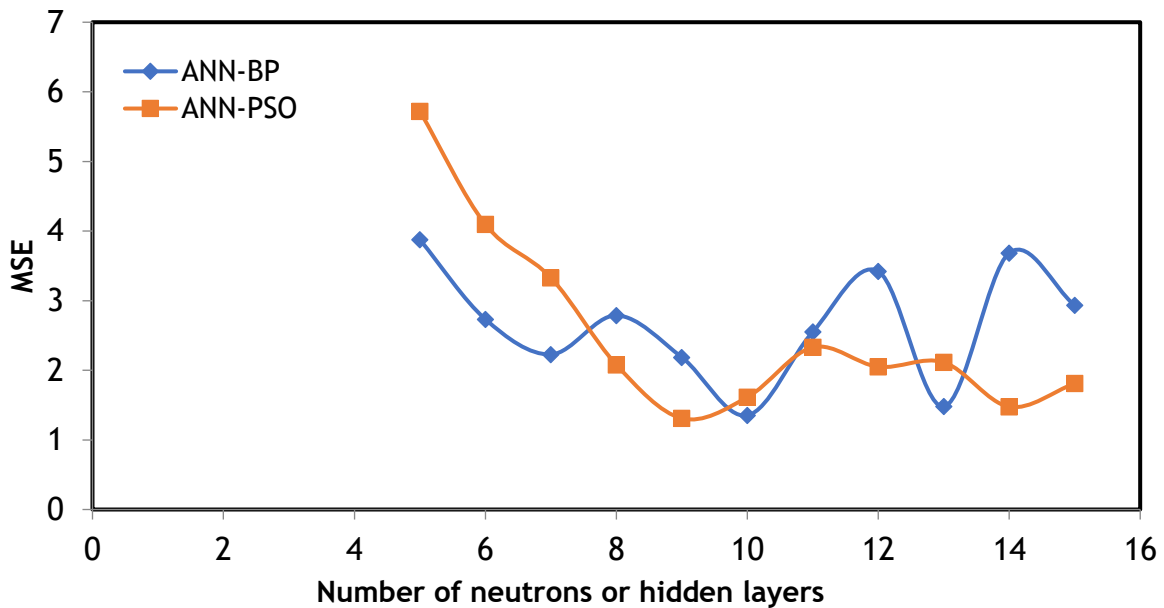


Figure 6: Mean square values against hidden layers

The regression plots give an insight of the anticipated outputs of any network after the training process. With regards to the training process, the coefficient of determination, R^2 , of 0.91054, 0.99994 and 0.99998 were obtained for the training, validation and test, respectively, with an overall average value of 0.96699, as shown in **Figure 7**. It is observed that the values are close to the 45° diagonal line, which indicates great proximity between the experimental and the network outputs.

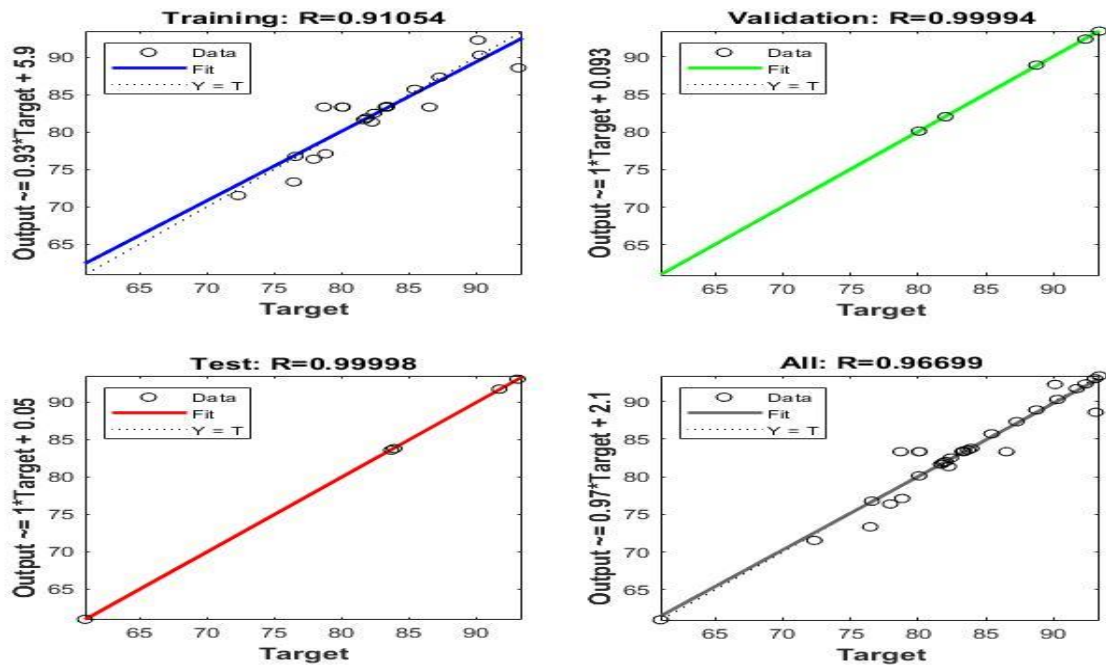


Figure 7: Regression plot of training, validation, test and average result

The weights and biases of the network of ANN is given in Table 6.

Table 6: Weights and biases of the network of ANN–BP algorithm

Neuron	1	2	3	4	5	6	7	8	9	10
Input 1 (Wi1)	-0.4625	-0.3591	6.2339	1.2553	2.7725	1.0138	0.7591	-5.2979	1.1132	-3.6926
2	2.7524	0.2375	-0.2930	-0.5076	2.531	3.0974	1.9416	-0.4805	2.6861	2.0504
3	1.5528	0.7349	1.7865	-0.0802	-3.1078	-2.6197	2.8457	1.3278	-0.3308	2.3517
4	-0.3721	-0.3446	-4.3995	-3.8004	2.5958	3.8917	-0.6956	2.5186	2.3	0.5859
5	1.2770	-0.9141	4.8591	-0.5848	4.3836	3.0893	-0.3946	-0.5363	0.5294	-2.3268
Output weights	0.5162	0.2232	3.2208	0.4397	0.9806	0.7909	0.6778	0.9321	-1.3784	-4.4076
Input bias, b_i	2.9735	3.98	-7.3803	-2.4152	-2.0183	-8.4738	1.8722	-3.3142	-0.4147	-4.2890
Output bias, b_j	0.2331									

The weights and biases consist of input layers and output layers for specific number of neutrons. The empirical equation can be developed from the weights and biases obtained from the network as expressed in Eqs. 7–9 taking cognisance of the activation functions.

$$y_{A-B} = \frac{2}{1 + e^{[-2 \times (0.5162F_1 + 0.2232F_2 + 3.2208F_3 + 0.4397F_4 + 0.9806F_5 + 0.7909F_6 + 0.6778F_7 + 0.9321F_8 - 1.3784F_9 - 4.4076F_{10})]}} - 1 \quad (7)$$

$$F_i = \frac{2}{1 + e^{-2E_i}} - 1, \quad i=1, 2, \dots, n \quad (8)$$

where n is the number of neurons.

$$E_i = w_{i1}x_1 + w_{i2}x_2 + w_{i3}x_3 + w_{i4}x_4 + w_{i5}x_5 + b_i \quad (9)$$

3.6 ANN–PSO Analysis

For the hybrid ANN–PSO algorithm, the hidden layers were varied between 5 and 15 neutrons to achieve the best trained network. As depicted in Figure 8, nine hidden layers gave the best network configuration with least MSE value of 1.31. This was achieved when c_1 is 1.5, c_2 is 2.5, w is 0.1350 within tolerance value of 0.0334 at maximum iteration of 1000. Figure 8 shows the regression plot of the trained hybrid algorithm with R^2 value of 0.98062. However, for the ANN–PSO algorithm, the weights and biases are presented in Table 7, and the empirical equation obtained is given in Eq. 10.

$$y_{A-P} = 0.6561 F_1 + 1.2984 F_2 + 1.0797 F_3 - 0.1287 F_4 + 1.1112 F_5 - 0.2659 F_6 - 0.7769 F_7 + 0.5135 F_8 - 0.6861 F_9 \quad (10)$$

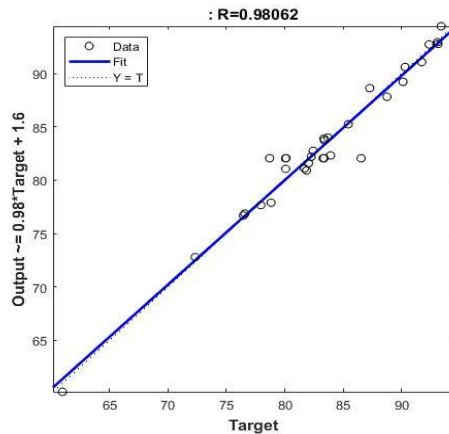
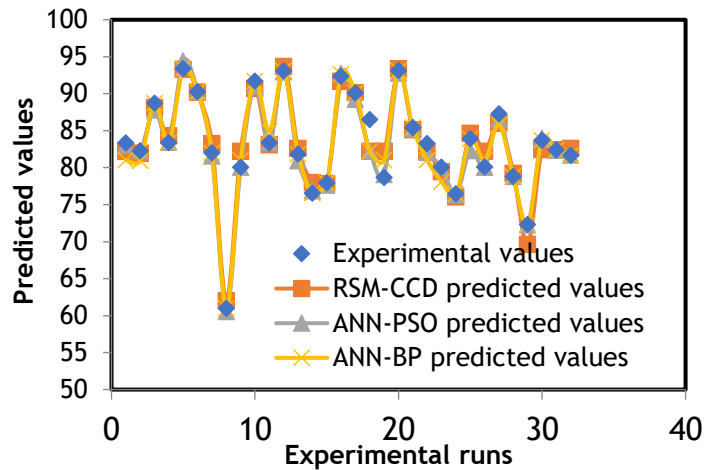
where $F_i = E_i$.

Table 7: Weights and biases of the network of ANN-PSO

Neuron	1	2	3	4	5	6	7	8	9
Input 1 (Wi1)	-1.500	-1.5000	0.478	-1.5000	0.1479	-1.5000	-1.5000	-1.5000	-0.2975
2	-0.5628	-1.5000	0.0269	-0.8231	0.6928	1.5000	0.3735	1.5000	-1.5000
3	0.6640	0.7156	-0.0216	1.5000	-1.500	-0.2085	-0.7427	-1.5000	-1.5000
4	0.7440	-1.4093	1.1186	1.5000	1.3998	1.5000	1.5000	1.5000	-1.1098
5	-1.5000	-0.3758	0.2873	1.5000	1.5000	1.5000	1.5000	1.5000	1.5000
Output weights	-0.6561	1.2984	1.0797	-0.1287	1.1112	-0.2659	-0.7769	0.5135	-0.6861
Input bias, b_i	1.500	0.3396	-1.500	1.0493	-0.0377	-1.5000	0.4226	-1.5000	-1.4733
Output bias, b_j	1.500								

3.7 Model comparison

The comparison between the experimental values and the predicted values of RSM-CCD, ANN-BP and ANN-PSO models are shown in **Figure 9**. Excellent agreements were achieved between the predicted and experimental values.

**Figure 8: Regression plot of trained hybrid ANN-PSO algorithm****Figure 9: Comparison of the experimental values of % removal of naphthalene with the RSM-CCD, ANN-BP and ANN-PSO predicted values**

To ascertain the accuracy of the models and evaluate the most fitted to the experimental values of % removal of naphthalene, the various error functions were used. **Table 8** shows the values of the error functions computed for the RSM-CCD, ANN-BP and ANN-PSO models. The results show clearly that ANN-PSO hybrid algorithm exhibits high generalization ability than RSM-CCD and ANN-BP algorithm due to the relatively low error functions' values obtained. The algorithm with the consistent lowest values depicts the most fitted (Yadav *et al.*, 2022).

3.8 Optimisation and validation

The PSO like other meta heuristic algorithms runs as a minimisation approach. For maximisation of the process variables, the objective function is an equivalent minimisation as given in Eq. 11.

$$J(\underline{x}) = \text{minimise}[1/y(\underline{x})] \quad (11)$$

where $J(\underline{x})$ is the objective function, \underline{x} the process variables solution vector ($= [A \ B \ C \ D \ E]^T$) and $y(\underline{x})$ the output from the network.

Table 8: Error functions' values of RSM-CCD, ANN-BP and ANN-PSO models

Error functions	Optimisation techniques		
	RSM-CCD	ANN-BP	ANN-PSO
R^2	0.9531	0.9671	0.9803
ARE	0.3114	0.2616	0.1997
$MPSD$	0.0098	0.0067	0.0038
$RMSE$	1.4122	1.2082	0.9364
χ^2	0.7941	0.5719	0.3382
$ERRSQ$	63.8214	46.7139	28.0646
$MAPE$	0.01246	0.0027	0.0040
MPE	1.2477	0.7573	0.5956
MAE	1.0094	0.6194	0.4971
$HYBRID$	0.7885	0.5580	0.3259
$EABS$	32.3000	19.8197	15.9970
ARD	1.2459	0.7453	0.5845
SEE	1.4585	1.2479	0.9672
SRE	1.4825	1.2113	0.8892
NSD	141.2239	120.8225	93.6475
SEP	1.6955	1.4506	1.1243

where R^2 the coefficient of determination, ARE the average relative error, $MPSD$ the Marquardt's percent standard deviation, χ^2 the normalized chi-square function, $ERRSQ$ the sum of error squares, $MAPE$ the mean absolute percentage error, MPE the mean percentage error, MAE the mean absolute error, $HYBRID$ the hybrid fractional error function, $EABS$ the sum of absolute errors, ARD the absolute relative deviation percent, SEE the standard error of estimate, SRE the standard deviation of relative error, NSD the normalized standard deviation, $RMSE$ the root mean square error, and SEP the standard error prediction.

The high and low values of the variables serve as the upper and lower bounds respectively. The parameters for optimisation include randomly initiated particles swarm size, $n(=100)$, acceleration coefficients or leaning constants, $c_1=2$ and $c_2=2$, initial and final weight values of $w_{min}=0.3$ and $w_{max}=0.9$ respectively for maximum iteration, $I_{max}=1000$. The weight, w , which controls how far a particle will move in a single iteration, I , that changes to improve the optimization performance is given in Eq. 12 (Narayanan *et al.*, 2023).

$$w = (w_{max} - w_{min}) \times \left(\frac{I_{max} - I}{I_{min}} \right) \quad (12)$$

The optimisation performance is reflected in the fitness value closely linked to MSE. The fitness function versus iteration plot is shown in **Figure 10**.

For the RSM-CCD technique, the design expert numerical optimisation option provides the optimum process variables for the developed Eq. 6 while the empirical Eqs. 7 and 10 for ANN-BP and ANN-PSO techniques respectively were optimized using the PSO algorithm. The results are presented in **Table 9**. The validation recorded percentage error of 0.602, 0.472 and 0.40 for RSM-CCD, ANN-BP and ANN-PSO respectively. This further gives ANN-PSO an edge over RSM-CCD and ANN-BP considered in this work.

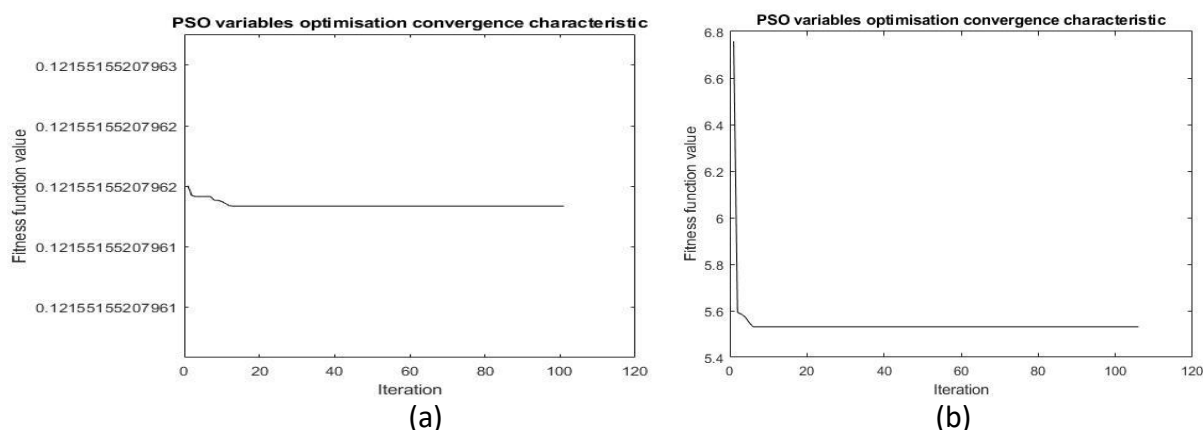


Figure 10: Fitness function and iteration plot for (a) ANN-BP, and (b) ANN-PSO

Table 9: Optimum condition, response and validation for the % removal of naphthalene

Process variables	<i>A</i> (mg/g)	<i>B</i> (g)	<i>C</i> (min)	<i>D</i> (°C)	<i>E</i>	Predicted Value	Validation Value
RSM-CCD	72.30	0.780	60.00	35.00	8.23	98.99	99.59
ANN-BP	75.00	0.25	75.00	35.00	7.00	99.10	99.57
ANN-PSO	75.00	0.25	75.00	30.00	11.00	99.96	100

4.0 CONCLUSION

In this study, optimization studies of naphthalene adsorption on bentonite clay-CTAB-chitosan matrix were carried out using RSM-CCD, ANN-BP and ANN-PSO techniques. The central composite design of experiment was carried out to investigate the effects of process variables on the % removal of naphthalene on the synthesized adsorbent matrix. The ANOVA results show that adsorbent dosage (*B*), temperature (*D*) and pH (*E*) are very significant while initial concentration (*A*) and contact time (*C*) were observed to be insignificant for the adsorption of naphthalene on the synthesized bentonite clay-cetyltrimethylammonium bromide (CTAB)-chitosan matrix. The interactive terms of initial concentration and adsorbent dosage (*AB*), adsorbent dosage and pH (*BE*); contact time and pH (*CE*), and temperature and pH (*DE*) give a synergistic effect on the adsorption process alongside the square terms of initial concentration (A^2), contact time (C^2), temperature (D^2) and pH (E^2). The RSM-CCD, ANN-BP and ANN-PSO adequately modelled the adsorption process of naphthalene on the synthesized matrix adsorbent. However, ANN-PSO shows superior generalisation ability when compared to that of RSM-CCD and ANN-BP on account of the values of the various error functions considered in addition to the percentage error of validation at the optimized process variables. The matrix of bentonite clay-cetyltrimethylammonium bromide (CTAB)-chitosan adsorbent can thus be effectively used to treat hydrophobic organic compounds. The limitation of this study is that the optimization studies carried out in this study are restricted to the adsorption of one of the recalcitrant PAHs (naphthalene) found in industrial wastewater. The adsorbent employed in this study is a hybrid of bentonite clay, CTAB, and chitosan from *Archachatina marginata* shell wastes. Hence, the results presented herein will not be applicable to other adsorbents, especially chitosan from other sources. Moreover, the model equations and optimum conditions obtained herein for percentage removal of naphthalene are inapplicable to other types of PAHs.

ACKNOWLEDGEMENTS

These are not applicable.

FUNDING

The authors declare that no funds, grants, or other support were received during the preparation of this manuscript.

AUTHORS' CONTRIBUTIONS STATEMENT

OAO: conceptualization, supervision, formal analysis, project administration, writing the original draft of the manuscript, critical review, expert view, and editing; VEB: literature review, methodology, formal analysis, validation of data, visualization of data, resources for data curation, and writing the original draft of the manuscript; OO, KOA, AMB and QOO: supervision, project administration, formal analysis, critical review, and visualization. All the authors contributed to the research article and approved the final version.

DATA AVAILABILITY

Datasets generated or analysed during the current study will be made available on request.

STATEMENTS & DECLARATIONS

ETHICAL

The current study did not include any human or animal subjects. Thus, this study is not subject to an ethics review committee and does not require any informed consent.

COMPETING INTERESTS

The authors declare that they have no known competing financial or non-financial interests or personal relationships that could have appeared to influence the work reported in this paper.

FINANCIAL INTERESTS

The authors have no relevant financial or non-financial interests to disclose.

REFERENCES

- ACGIH – American Conference of Governmental Industrial Hygienists (2010) Threshold limit values and biological exposure indices. ACGIH, Cincinnati, OH.
- Afroozeh, M., Sohrabi, M. R., Davallo, M., Mirnezami, S. Y., Motiee, F. and Khosravi, M. (2018). Application of artificial neuro-fuzzy inference system to predict the removal of Pb (II) ions from the aqueous solution by using magnetic graphene/nylon 6. *Chemical Sciences Journal*, 9: 1–7. <https://doi.org/10.4172/2150-3494.10001.185>
- Agarry, S. E., Ogunleye, O. O. and Aworanti, O. A. (2013). Biosorption equilibrium, kinetic and thermodynamic modelling of naphthalene removal from aqueous solution onto modified spent tea leaves. *Environmental Technology*, 34: 825–839. <https://doi.org/10.1080/09593330.2012.720616>
- Al-Alam, J., Lévy, M., Ba, H., Pham-Huu, C. and Millet, M. (2020). Passive air samplers based on ceramic adsorbent for monitoring of organochlorine pesticides, polycyclic aromatic hydrocarbons and polychlorinated biphenyls in outdoor air. *Environmental Technology & Innovation*, 20: 101094. <https://doi.org/10.1016/j.eti.2020.101094>
- Al-Alam, J., Millet, M., Khoury, D., Rodrigues, A., Akoury, E., Tokajian, S. and Wazne, M. (2024). Biomonitoring of PAHs and PCBs in industrial, suburban, and rural areas using snails as sentinel organisms. *Environmental Science and Pollution Research*, 31: 4970–4984. <http://doi.org/10.1007/s11356-023-31493-6>
- Albayati, T. M. and Kalash, K. R. (2020). Polycyclic aromatic hydrocarbons adsorption from waste water using different types of prepared mesoporous materials MCM-41 in batch and fixed bed column. *Process Safety and Environmental Protection*, 133: 124–136. <https://doi.org/10.1016/j.psep.2019.11.007>
- Alharbi, H. A., Alotaibi, K. D., El-Saeid, M. H. and Giesy, J. P. (2023). Polycyclic aromatic hydrocarbons (PAHs) and metals in diverse biochar and products: effects of feedstock type and pyrolysis temperature. *Toxics*, 11: 1–15. <https://doi.org/10.3390/toxics11020096>
- Alizamir, M. and Sobhanardakani, S. (2018). An artificial neural network-particle swarm optimization (ANN-PSO) approach to predict heavy metals contamination in ground resources. *Jundishapur Journal of Health Sciences*, 1–8. <https://doi.org/10.5812/jjhs.67544>
- Al-Salman, A. N., Al-Niaeem, K. S. and A-Ghizzawi, G. J. (2023). Polycyclic aromatic hydrocarbons (PAHs) in sediment and the health risk to fish in the Shatt Al-Arab River, Basrah, Iraq. *Research in Veterinary Science*, 155: 1–23.

- Arikan, B., Konakci, C. O., Yildiztugay, E., Turan, M. and Cavusoglu, H. (2022). Polystyrene nanoplastic contamination mixed with polycyclic aromatic hydrocarbons: Alleviation on gas exchange, water management, chlorophyll fluorescence and antioxidant capacity in wheat. *Environmental Pollution*, 311: 119851. <http://doi.org/10.1016/j.envpol.2022.119851>
- Asadu, C. O., Ekwueme, B. N., Onu, C. E., Onah, T. O., Ike, I. C. and Ezema, C. A. (2022). Modelling and Optimization of crude oil removal from surface water via organic acid functionalized biomass using machine learning approach. *Arabian Journal of Chemistry*, 15: 1–21. <https://doi.org/10.1016/j.arabjc.2022.104025>
- Asfaram, A., Ghaedi, M., Azghandi, A. M. H., Goudarzi, A. and Dastkhoon, M. (2016). Statistical experimental design, least square-support vector machines (LS-SVM) and artificial neural network (LS-SVM) and artificial neural network (NN) models for modelling the facilitated adsorption of methylene blue dye. *RSC Advances*, 6: 40502–40516. <https://doi.org/10.1039/cbra01874b>
- Atemkeng, C. D., Anagho, G. S., Tagne, R. F. T., Amola, L. A., Bopda, A. and Kamgaing, T. (2021). Optimization of 4-nonylphenol adsorption on activated carbons derived from Safou seeds using response surface methodology. *Carbon Trend*, 4: 100052. <https://doi.org/10.1016/y.cartre.2021.100052>
- Avila, H. E. R., Villarreal, I. A. A., Munoz, L. L. D., Perez, J. M., Pruiz, F. J. S., Mayorga, C. K. R., Castillo, D. I. M. and Petriciolet, A. B. (2022). A review of the modelling of adsorption of organic and inorganic pollutants from water using artificial neural networks. *Adsorption Science and Technology*, 2022: 1–51. <https://doi.org/10.1155/2022/9384871>
- Azeez, S. O., Jimoh, A. A., Saheed, I. O., Otun, K. O., Mustapha, A. O. and Adekola, F. A. (2022). Optimization by Box Behnken design for Eosin yellow dye removal from aqueous medium using data palm seeds-porous carbon @ TiO₂ blend. *Journal of Nigerian Society of Physical Sciences*, 4: 183–192. <http://dx.doi.org/10.46481/jnsps.2022.533>
- Azhar-ul-Haq, M., Javed, T., Abid, M. M., Masood, H. T. and Muslim, N. (2022). Adsorptive removal of hazardous crystal violet dye onto banana peel powder: equilibrium, kinetic and thermodynamics studies. *Journal of Dispersion Science and Technology*, 1–16. <https://dx.doi.org/10.1080/01932691.2022.2158851>
- Balati, A., Shahbazi, A., Amini, M. M. and Hashemi, S. H. (2015). Adsorption of polycyclic aromatic hydrocarbons from waste water by using silica-based organic-inorganic nanohybrid material. *Journal of Water Reuse and Desalination*, 5: 1–14. <https://doi.org/10.2166/wrd.2014.013>
- Batchamen Mougno, J. B., Waanders, F., Ntwampe, S. K. O., Fosso-Kankeu, E. and Al Alili, A. R. (2022). Synthesis of eco-friendly ZnO-based heterophotocatalysts with enhanced properties under visible light in the degradation of organic pollutants. *Environmental Systems Research*, 11(25): 25. <https://doi.org/10.1186/s40068-022-00271-7>
- Bello, V. E. and Olafadehan, O. A. (2021). Comparative investigation of RSM and ANN for multi-response modeling and optimization studies of derived chitosan from *Archachatina marginata* shell, *Alexandria Engineering Journal*, 60(4): 3869–3899. <https://doi.org/10.1016/j.aej.2021.02.047>
- Bieda, A. F., Pereee, A. and Zalas, A. R. (2023). Modelling and optimization of Geraniol ((2E)-3,7-dimethyl-2,6-cctadiene-1-ol) transformation process using response surface methodology (RSM). *Catalysts*, 13: 1–16. <https://dx.doi.org/10.3390/catal13020320>
- Chitto, B. S. and Sutherland, C. (2020). Column breakthrough studies for the removal and recovery of phosphate by lime-iron sludge: modeling and optimization using artificial neural network and adaptive neuro-fuzzy inference system. *Chinese Journal of Chemical Engineering*, 28(7):1847–1859. <https://doi.org/10.1016/j.cjche.2020.02.02>
- da Costa, T. B., da Silva, T. L., Costa, C. S. D., da Silva, M. G. C. and Vieira, M. G. A. (2022). Chromium adsorption using *Sargassum filipendula* algae waste from alginate extraction: batch and fixed-bed column studies. *Chemical Engineering Journal Advances*, 11: 100341. <http://doi.org/10.1016/j.cej.2022.100341>
- Dahlan, I., Azhar, E. E. M., Hassan, S. R., Aziz, H. A. and Hung, Y. T. (2022). Statistical modelling and optimization of process parameters for 2,4-dichlorophenoxyacetic acid removal by using ac/pdmaema hydrogel adsorbent: comparison of different RSM designs and ANN training methods. *Water*, 14: 1–17. <https://doi.org/10.3390/w14193061>
- Danesh, N., Ghorbani, M. and Marjani, A. (2021). Separation of copper ions by nano-composites using adsorption process. *Scientific Reports*, 11: 1–23. <https://doi.org/10.1038/s41598-020-80914-w>
- Darwish, M. S. A., Mostafa, M. H. and Al-Harbi, L. M. (2022). Polymeric nanocomposites for environmental and industrial applications. *International Journal of Molecular Sciences*, 23: 1023. <http://doi.org/10.3390/ijms23031023>
- Domgas, R., Dauda, A., Arnand, M. A. G., Balike, M., Bagamla, W. and Bosco, T. J. (2023). Optimization of methylene blue adsorption onto activated carbon from Bos Indicus Gudali bones using a Box Behnken Experimental design. *Journal of the American Chemical Society*, 12: 1–9. <https://doi.org/10.5923/j.chemistry.20221201.01>

- Eberhart, R. C. and Kennedy, J. (1995). A new optimizer using particle swarm theory. *Proceedings of the Sixth International Symposium on Micro Machine and Human Science*, 1: 39–43. <http://dx.doi.org/10.1109/MHS.1995.494215>
- El-Hanandeh, A., Zainab, M. and Imtiaz, M. S. (2021). Modelling of the adsorption of Pb, Cu and Ni ions from single and multi-component aqueous solutions by date seed derived biochar: comparison of six machine learning approaches. *Environmental Research*, 192: 110338. <https://doi.org/10.1016/j.enres.2020.110338>
- El-Shorbagy, M. A. and Hossaniem, A. E. (2018). Particle swarm optimization from theory to applications. *Int J Rough Sets Data Anal* 5:1–24. <https://doi.org/10.4018/IJRSDA.2018040101>
- El-Zahhar, A. A. and Idris, A. M. (2022). Synthesis, characterization, and application of TiO₂–magnetite/chitosan nanocomposite for adsorptive removal of naphthalene from aqueous solutions. *Petroleum Chemistry*. 62: 788–799. <https://doi.org/10.1134/S0965544122010066>
- Emezie, N. E., Etuk, B. R., Akpan, O. P. and Chiweoke, O. C. (2022). Cyanide removal from cassava wastewater onto H₃PO₄ activated periwinkle shell carbon. *Applied Water Science*, 12: 1–12. <https://doi.org/10.1007/s13201-022-01679-3>
- Emoyan, O. O., Agbaire, P. O., Otobrise, C. and Akporhonor, E. E. (2011). Distribution pattern of polyaromatic hydrocarbon (PAHs) in soils in the vicinity of fuel stations in Abraka, Nigeria. *Journal of Applied Sciences and Environmental Management*, 15: 513–516
- Faisal, A. A., Ramadhan, Z. K., Al-Ansari, N., Sharma, G., Naushad, M. and Bathula, C. (2022). Precipitation of (Mg/Fe-CTAB)-layered double hydroxide nanoparticles onto sewage sludge for producing novel sorbent to remove Congo red and methylene blue dyes from aqueous environment. *Chemosphere*, 291: 132693. <https://doi.org/10.1016/j.chemosphere.2021.132693>
- Frescura, L. M., de Menezes, B. B., Duarte, R. and da Rosa, M. B. (2020). Application of multivariate analysis on naphthalene adsorption in aqueous solutions. *Environmental Science and Pollution Research*, 27: 3329–3337. <https://doi.org/10.1007/s11356-019-07278-1>
- Ganesapillai, M., Sinha, A., Mehta, R., Tiwari, A., Chellappa, V. and Drewnowski, J. (2022). Design and analysis of artificial neural network (ANN) models for achieving self-sustainability in sanitation. *Applied Sciences*, 12: 1–21. <https://doi.org/10.3390/app12073384>
- Garbal, Z. N., Ekwumemgbo, P. A. and Stephen, G. (2022). Optimization of phenol adsorption from synthetic waste water by synthesized BiFeO₃ perovskite material using split-plot central composite design. *Bulletin of the National Research Centre*, 46: 1–14. <http://doi.org/10.1186/s42269-022-00866-1>
- Gil, A., Santamaria, L., Korili, S. A., Vicente, M. A., Barbosa, L. V., de Souza, S. D., Marcel, L., de Faria, E. H. and Ciuffi, K. J. (2021). A review of organic-inorganic hybrid clay-based adsorbents for contaminants removal: synthesis, perspectives and applications. *Journal of Environmental Chemical Engineering*, 9: 1–18. <https://doi.org/10.1016/j.jece.2021.105808>
- Gong, C., Huang, H., Qian, Y., Zhang, Z. and Wu, H. (2017). Integrated electrocoagulation and membrane filtration for PAHs removal from realistic industrial waste water: effectiveness and mechanisms. *The Royal Society of Chemistry Advances*, 7: 52366–52374. <https://doi.org/10.1039/C7ra09372a>
- Hussain, M. S., Rehman, R. and Imran, M. (2022). Comparative evaluation of the adsorption performance of citric acid treated peels of *Trapa natans* and *citrullus lanatus* for cationic dyes degradation from water. *Journal of Chemistry*, 2022: 1109376. <https://doi.org/10.1155/2022/1109376>
- Ike, I. S., Asadu, C. O., Ezema, C. A., Onah, T. O., Ogbodo, N. O., Nwakwasi, E. U. G. and Onu, C. E. (2022). ANN-GA, ANFIS-GA and thermodynamics base modelling of crude oil removal from water surface using organic acid grated banana pseudo stem fiber. *Applied Surface Science Advances*, 9: 1–13. <https://doi.org/10.1016/j.apsadv.2022.100259>
- Ivwurie, W. and Okiriguo, D. (2022). Evaluation of polycyclic aromatic hydrocarbon from selected communities in Udu local government area of Delta state. *FUPRE Journal of Scientific and Industrial Research*, 6: 1–11.
- Karri, R. R. and Sahu, J. N. (2018). Modeling and optimization by particle swarm embedded neural network for adsorption of zinc (II) by palm kernel shell based activated carbon from aqueous environment. *J Environ Manage* 206:178–191. <https://doi.org/10.1016/j.jenvman.2017.10.026>
- Kim, U. J., Saito, N. and Lee, S. H. (2022). Remediation of water contamination with polycyclic aromatic hydrocarbons using liquid phase plasma: influence of electrical discharge condition. *Frontier in Marine Science*, 9: 1–12. <https://dx.doi.org/10.3389/fmars.2022.1033962>
- Law, S. K., Fung, Y. H., Chan, H. Y., Han, J. and Lo, C. M. (2022). A mini-review for an adsorption of polycyclic aromatic hydrocarbons (PAHs) by physical gel. *Biointerface Research in Applied Chemistry*, 12: 8195–8204. <https://doi.org/10.33263/BRIAC126.81958204>
- Li, H., Budarin, V. L., Clark, J. H., North, M. and Wu, X. (2022). Rapid and efficient adsorption of methylene blue dye from aqueous solution by hierarchically porous, activated starbons®: Mechanism and porosity dependence. *Journal of Hazardous Materials*, 436: 1–16. <https://doi.org/10.1016/j.jhazmat.2022.129174>

- Llyas, M., Ahmad, W. and Khan, H. (2021). Utilization of activated carbon derived from waste plastic for decontamination of polycyclic aromatic hydrocarbons laden waste water. *Water Science & Technology*, 84: 609–631. <https://doi.org/10.2166/Wst.2021.252>
- Manyangadze, M., Chikuruwo, N. H. M., Narsaiah, T. B., Chakra, C. S., Radhakumari, M. and Danha, G. (2020). Enhancing adsorption capacity of nano-adsorbents via surface modification: A review. *South African Journal of Chemical Engineering*, 31: 25–32. <https://doi.org/10.1016/j.sajce.2019.11.003>
- Moreno, R. S. and Salazar, Z. (2018). An artificial neural network model to analyze maize price behaviour in Mexico. *Applied Mathematics*, 9: 473–487. <https://doi.org/10.4236/am.2018.95034>
- Nagababu, A., Reddy, D. S. and Mohan, G. V. K. (2022). Toxic chrome removal from industrial effluents using marine algae: modelling and optimization. *Journal of Industrial & Engineering Chemistry*, 114: 337–390. <https://doi.org/10.1016/j.jiec.2022.07.027>
- Narayanan, S. L., Kasiselvanathan, M., Gurumoorthy, K. B. and Kiruthika, V. (2023). Particle swarm optimization based artificial neural network (PSO-ANN) model for effective k-barrier count intrusion detection system in WSN. *Measurement: Sensors*, 29: 1–6. <https://doi.org/10.1016/j.measen.2023.100875>
- Nayagam, J. O. P., Prasanna, K. and Kumar, P. S. (2023). Effective separation of toxic azo dyes from water system using the activated carbon derived from *Prosopis juliflora* roots. *Desalination & Water Treatment*, 285: 242–263. <https://doi.org/10.5004/dwt.2023.29216>
- Nguyen, T. T. T., Hoang, D. Q., Nguyen, D. T. C. and Tran, T. V. (2022). Adsorptive optimization of crystal violet dye using central composite rotatable design and response surface methodology: statistical analysis, kinetic and isotherm studies. *Arabian Journal for Science & Engineering*, 1:1–14. <https://doi.org/10.1007/s13369-022-07391-3>
- NMAM (NIOSH Manual of Analytical Methods) (2019) Polycyclic aromatic hydrocarbon by GC: methods 5515. 4th ed., U.S. Department of Health, Education, and Welfare.
- Okoji, A., Ambrose, A., James, O., Abiola, T. and Osuolale, F. (2021). Energetic assessment of a precalcining rotary kiln in a cement plant using simulator and neural networks. *Alexandria Engineering Journal*, 61(7): 5097–5109. <https://doi.org/10.1016/j.aej.2021.010>
- Okoro, H. K., Tella, A. C., Ajibola, O. A., Zvinowanda, C. and Ngila, J. C. (2019). Adsorptive removal of naphthalene and anthracene from aqueous solution with zinc and copper-terephthalate metal-organic frame works. *Bulletin of the Chemical Society of Ethiopia*, 33: 229–241. <https://doi.org/10.4314/bese.v33i2.4>
- Olafadehan, O. A., Aminu, F. U., Adewunmi, O. V., Kabiawu, A. I., Akinyanju, A. S., Amokun, M. K., Bello, A. M. and Olafadehan, Q. O. (2025). Isothermic, kinetic and thermodynamic studies of chromium (VI) ions adsorption on composite adsorbent of chitosan-eggshell activated carbon. *Petroleum & Petrochemical Engineering Journal*, 9: 1–34. <https://doi.org/10.23880/ppej-16000408>
- Olafadehan, O. A. and Bello, V. E. (2022). Comparative Studies of RSM, RSM-GA and ANFIS for modelling and optimization of naphthalene adsorption on chitosan-CTAB-sodium bentonite clay matrix. *Journal of Applied Science & Process Engineering*, 9(1): 1242–1280. <http://doi.org/10.33736/jaspe.4749.2022>
- Olafadehan, O. A., Bello, V. E. and Adesina, A. J. (2023). ANN optimization of adsorption of naphthalene on composite nanoparticles of chitosan-CTAB-sodium bentonite clay. *Petroleum & Petrochemical Engineering Journal*, 7(2): 000354. <http://doi.org/10.23880/ppej-16000354>
- Olafadehan, O. A., Bello, V. E. and Amoo, K. O. (2022). Production and characterization of composite nanoparticles derived from chitosan, CTAB and bentonite clay. *Chemical Papers*, 76:5063–5086. <https://doi.org/10.1007/s11696-022-02228-7>
- Onukwuli, O. D. and Nnanwube, I. A. (2022). Optimization of zinc recovery from sphalerite using response surface and particle swarm optimization. *Periodica Polytechnica Chemical Engineering*, 66: 20–29. <https://doi.org/10.3311/PPch.17897>
- Peng, X., Du, P. F., Tang, H., Meng, Y., Yuan, L. and Sheng, L. P. (2018). Degradation of polycyclic aromatic hydrocarbons: a review. *Applied Ecology and Environmental Research*, 16: 6419–6440. http://dx.doi.org/10.15666/acer/1605_64196440
- Prabhakar, M., Gomathi, K., Venkatesh, R., Stalany, V. M., Vijayan, D. S., Sassykova, L. R., Sendilvalan, S., Priya, V. S., Jijina, G. O. and Selvaraj, R. (2022). Isothermic and kinetic study on removal of methylene blue dye using anisomeles malabaricus silver nanoparticles: an efficient adsorbent to purify dye-contaminated waste water. *Adsorption Science & Technology*, 2022: 1–7. <https://doi.org/10.1155/2022/9878987>
- Puszkarewicz, A. and Kaleta, J. (2020). The efficiency of the removal of naphthalene from aqueous solutions by different adsorbents. *Int J Environ Res Public Health* 17:1–16. <https://doi.org/10.3390/ijerph17165969>
- Queiroz, R. N., da Silva, M. G. C., Mastelaro, V. R., Prediger, P. and Vieira, M. G. A. (2023). Adsorption of naphthalene polycyclic aromatic hydrocarbon from waste water by a green magnetic composite based on chitosan and grapheme oxide. *Environmental Science and Pollution Research International*, 30: 27603–27621. <https://doi.org/10.1007/s11356-022-24198-9>

- Raaj, E. P., Bhuvaneshwari, K., Lakshmipathy, R., Devi, V. V. and Rico, I. L. R. (2022). Garlic peel surface modification and fixed column investigations towards crystal violet dye. *Adsorption Science and Technology*, 2022:1–9. <http://dx.doi.org/10.1155/2022/6904842>
- Radoor, S., Karayil, J., Jayakumar, A., Parameswaranpillai, J., Lee, J. and Siengchin, S. (2022). Ecofriendly and low-cost bio adsorbent for efficient removal of methylene blue from aqueous solution. *Scientific Report*, 12:20580. <https://doi.org/10.1038/s41598-022-22936-0>
- Rosinska, A. and Dabrowska, L. (2018). Selection of coagulants for the removal of chosen PAHs from drinking water. *Water*, 10: 1–14. <https://doi.org/10.3390/w10070886>
- Rossides, G., Metcalfe, B. and Hunter, A. (2021). Particle swarm optimization – An adaptation for the control of robotic swarms. *Robotics*, 10: 58. <https://doi.org/10.3390/robotics10020058>
- Sabah, E. and Ouki, S. (2017). Adsorption of pyrene from aqueous solutions onto sepiolite. *Clays and Clay Minerals*, 65: 14–26. <https://doi.org/10.1346/CCMN.2016.064046>
- Satouh, S., Martín, J., del Mar Orta, M., Medina-Carrasco, S., Messikh, N., Bougdah, N., Santos, J. L., Aparicio, I. and Alonso, E. (2021). Adsorption of polycyclic aromatic hydrocarbons by natural, synthetic and modified clays. *Environments*, 8: 124. <https://doi.org/10.3390/environments8110124>
- Satyobroto, T. (2011). Mathematical modelling and applications of particle swarm optimization. MA Thesis. Blekinge Institute of Technology.
- Sayed, M. A., Aly, H. F., Mahmoud, H. H., Abdelwahab, S. M., Heiai, A. F. I. and Wilson, I. D. (2022). Synthesis and characterization of hausmannite-activated carbon nanocomposites for removal of lead from aqueous solutions. *Chemical Engineering & Technology*, 45: 717–726. <http://dx.doi.org/10.1002/ceat.202100365>
- Shariati, M., Mafipour, M. S., Mehrabi, P., Bahadori, A., Zandi, Y., Salih, M. N. A., Nguyen, H., Dou, J., Song, X. and Ngian, S. P. (2019). Application of a hybrid artificial neural network-particle swarm optimization (ANN-PSO) model in behavior prediction of channel shear connectors embedded in normal and high-strength concrete. *Applied Sciences*, 9: 1–22. <http://doi.org/10.3390/app9245534>
- Soltani, R., Marjani, A. and Shirazian, S. (2019). Facile one-pot synthesis of thiol-functionalized mesoporous silica submicrospheres for Tl(I) adsorption: isotherm, kinetic and thermodynamic studies. *Journal of Hazardous Materials*, 371: 146–155. <https://doi.org/10.1016/j.jhazmat.2019.02.076>
- Suresh, S., Kuman, P., Jha, J. M., Verma, S., Arisutha, S. and Lens, P. N. (2022). Sonocatalytic removal of naphthalene from an aqueous solution using ZnO nanoparticles. *AQUA Water Infrastructure, Ecosystems and Society*, 71: 1002–1015. <https://doi.org/10.2166/aqua.2022.042>
- Tai, Y. K., Sim, L. C., Leong, K. H. and Saravanan, P. (2021). Optimization study of adsorption parameters for removal of dye pollutant using candle soot coated egg carton. *IOP Conference Series: Earth and Environmental Science*, 945: 1–8. <https://doi.org/10.1088/1755-1315/945/1/012012>
- Taiwo, O. C., Afolabi, T. J., Osuolale, F. N., Ajani, A. O., Aworanti, O. A., Ogunleye, O. R. and Alade, A. O. (2021). Recycling of waste expanded polystyrene as an effective adsorbent of naphthalene from aqueous solution. *Kemija u industriji/J Chemists and Chemical Engineers*, 70: 519–534. <https://doi.org/10.15255/KUI.2020.084>
- Tentori, E. F., Ashenafi, E. L., Urshel, M. R. and Nyman, M. C. (2021). Peroxy-acid treatment of polycyclic aromatic hydrocarbons: degradation kinetics, thermodynamics and predictive modelling. *Journal of Environmental Engineering*, 147: 0421053. [https://doi.org/10.1061/\(ASCE\)EE.1943-7870.0001924](https://doi.org/10.1061/(ASCE)EE.1943-7870.0001924)
- Urbano, L. G., Guzman, M. V., Recuerda, R. P. and Rodriguez, J. M. (2021). Removal of polycyclic aromatic hydrocarbons (PAHs) in convectional drinking water treatment processes. *Journal of Contaminant Hydrology*, 243: 1–7. <https://doi.org/10.1016/j.jconhyd.2021.103888>
- Wang, R., Zhong, M., Li, W., Chen, Y., Tan, Z., Li, X. and Zhang, J. (2022). Isotherm and kinetic studies of biosorption of low concentration Cr (III) from aqueous solution by 4 microbial biosorbents. *Polish Journal of Environmental Studies*, 31: 1363–1376. <https://doi.org/10.15244/pjoes/141903>
- Xu, Q., Liu, T., Li, L., Liu, L., Liu, B., Wang, X., Zhang, S., Li, L., Wang, B., Zimmerman, A. R. and Gao, B. (2021). Hydrothermal carbonization of distillers grains with clay minerals for enhanced adsorption of phosphate and methylene blue. *Bioresource Technology*, 340: 125725. <https://doi.org/10.1016/j.biortech.2021.125725>
- Yadav, A. and Roy, S. M. (2023). An artificial neural network-particle swarm optimization (ANN-PSO) approach to predict the aeration efficiency of venturi aeration system. *Smart Agricultural Technology*, 4: 1–9. <https://doi.org/10.1016/j.atech.2023.100230>
- Yadav, D. K., Kumar, A. R., Jayaraman, S., Lenka, S., Gurjar, S., Sarkar, A., Saha, J. K. and Patra, A. K. (2022). Polycyclic aromatic hydrocarbons in diverse agricultural soils of central India: occurrences, sources, and potential risks. *International Journal of Environmental Analytical Chemistry*, 1–15. <http://doi.org/10.1080/03067319.2022.2125307>
- Yakout, S. M., Daifullah, A. A. M. and Reefy, S. A. (2013). Adsorption of naphthalene, phenanthrene and pyrene from aqueous solution using low cost activated carbon derived from agricultural wastes. *Adsorption Science & Technology*, 31: 293–302.

- Yemele, O. M., Zhao, Z., Nkoh, J. N., Ymele, E. and Usman, M. (2024). A systematic review of polycyclic aromatic hydrocarbon pollution: A combined bibliometric and mechanistic analysis of research trend toward an environmentally friendly solution. *Science of The Total Environment*, 926: 171577. <https://doi.org/10.1016/j.scitotenv.2024.171577>
- Yeo, J. Y. J., Khaerudini, D. S., Soetaredjo, F. E., Waworuntu, G. L., Ismadji, S., Putranto, A. and Sunarso, J. (2023). Experimental and modelling study of adsorption isotherms of amoxicillin, ampicillin and doripenem on bentonite-chitosan composite. *South African Journal of Chemical Engineering*, 43: 38-45. <https://doi.org/10.1016/j.sajce.2022.09.013>
- Zango, Z. U., Jumbri, K., Sambudi, N. S., Bakar, N. H. H. A., Adullah, N. A. F., Basheer, C. and Saad, B. (2019). Removal of anthracene in water by MIL-88 (Fe), NH₂-MIL-88(Fe), and mixed-MIL-88(Fe) metal-organic frame works. *The Royal Society of Chemistry Advances*, 9: 41490–41501. <https://doi.org/10.1039/c9ra0860a>
- Zhao, W., Hao, C., Guo, Y., Shao, W., Tian, Y. and Zhao, P. (2023). Optimization of adsorption conditions using response surface methodology for tetracycline removal by MnFe₂O₄/multi-wall carbon nanotubes. *Water*, 15:2392. <https://doi.org/10.3390/w15132392>
- Zulaihah, L., Marasabessy, A. and Sari, S. (2020). The experiment test of absorbents for controlling poly aromatics hydrocarbon on sea water around gravity dock and hhip loading terminal. *IOP Conference Series: Materials Science and Engineering*, 1125: 1–8. <https://dx.doi.org/10.1088/1757-899X/1125/1/012110>